



Immune particle swarm optimization of SUV rollover crashworthiness and weight

Zhilin Jin¹ · Senhao Zhang¹ · Jiansheng Weng¹

Received: 18 November 2020 / Revised: 28 February 2021 / Accepted: 16 March 2021 / Published online: 6 April 2021
© The Author(s), under exclusive licence to Springer-Verlag GmbH Germany, part of Springer Nature 2021

Abstract

When designing a sport utility vehicle (SUV), designers strive to improve the vehicle's rollover crashworthiness while avoiding a significant increase in its weight. To aid in optimizing such a trade-off, this paper proposes a multi-disciplinary and multi-objective hybrid optimization algorithm that combines particle swarm optimization and the artificial immune method. First, the SUV structure's influence on body mass and rollover crashworthiness is studied using contribution analysis, and structural improvements are discussed according to Federal Motor Vehicle Safety Standard 216. Building on the analysis results, the SUV's rollover crashworthiness and weight optimization model are proposed. Radial basis function neural network and a genetic algorithm are used to build and optimize surrogate models of total weight, maximum contact force, and torsion frequency. The proposed algorithm then utilizes particle swarm and artificial immune to seek Pareto solutions that optimize SUV structure. Finally, the technique for order preference by similarity to ideal solution method determines a final solution from Pareto-optimal solutions. Compared to previous studies, the results show that the proposed hybrid optimization algorithm improves the Pareto solution sets' diversity and distribution uniformity, enhances SUV rollover crashworthiness, and reduces SUV structure components' weight.

Keywords SUV rollover crashworthiness · Weight reduction · Material structure integrated design · Multi-disciplinary and multi-objective optimization · Hybrid optimization algorithm

1 Introduction

In automotive design, safety is essential. Although vehicle rollovers are relatively rare, their casualty rate is very high compared with other collision accidents (George et al. 1996). According to the National Highway Traffic Safety Administration (NHTSA) statistics for Administration 2018, there were more than 6 million vehicle crashes in the USA, including more than 48 thousand vehicle rollovers. In total, vehicle rollovers caused 17.9% of all crash fatalities (NHTSA 2018). Large vehicles and sport utility vehicles (SUVs) are especially prone to rollover due to centroid height. The SUV's rollover rate is more than nine times that of cars, and

the chance of casualties is much higher (Mohammad et al. 2019). Consequently, the SUV's passive safety improvement has become an important research topic (Bai et al. 2019; Trajkovski et al. 2018). In addition, the severity of environmental pollution prompted studies on vehicle emission reduction through a decrease in vehicles' weight (Zhu et al. 2009; Gunddolf et al. 2012). Thus, SUVs' rollover crashworthiness improvement and weight minimization emerged as a critical trade-off.

Numerous studies are aimed at simultaneous crashworthiness improvement and weight reduction. Cui et al. (2011) optimized the material combinations for 20 body structures, improving the front collision crashworthiness and reducing the body mass by 30.9 kg. Xiong et al. (2018) employed a contribution analysis to detect impactful body parts in head-on collisions. The authors used particle swarm optimization to improve crashworthiness and reduce body weight and production costs. Kiani et al. (2014) selected 22 vehicle parts as design variables and formulated a mass minimization problem under crash and vibration constraints. The problem was then solved using sequential quadratic programming. Lee

Responsible Editor: Gengdong Cheng

✉ Zhilin Jin
jinzhilin@nuaa.edu.cn

¹ Department of Vehicle Engineering, Nanjing University of Aeronautics and Astronautics, Nanjing 210016, China

et al. (2018) studied the relationship between side-impact crashworthiness and B-pillar topology in a vehicle rollover. As a result, the authors proposed an optimized B-pillar that does not significantly diminish the crashworthiness but reduces the pillar's weight. Choi et al. (2018) analyzed the SUV's top and side structures' crashworthiness and found that it deviates from the Federal Motor Vehicle Safety Standard (FMVSS) 216. The conducted optimization considered several structures' dimensions as variables, maximum contact force as a constraint, and weight as the objective.

Vehicle collision is a typical nonlinear problem. Since traditional optimization algorithms perform poorly on such nonlinear, complex problems, researchers often rely on intelligent optimization algorithms to tackle vehicle collision optimization problems (Perez and Behdinan 2007; Gu et al. 2013; Khalkhali et al. 2014). One of the most popular global optimization methods is particle swarm optimization (PSO) (Kennedy and Eberhart 1995). However, PSO is prone to falling in local optima and may result in a non-uniform solution distribution. Another popular optimization algorithm is the non-dominated sorting genetic algorithm (NSGA) – II (Deb et al. 2000). Due to its speed and good convergence properties, NSGA-II became a benchmark multi-objective optimization algorithm. (Hou et al. 2014) utilized NSGA-II for multi-objective optimization of vehicle body's side parts. Wang et al. (2016a) considered the subframe's weight, first-order natural frequency, and maximum stress as three conflicting objective functions. The improved NSGA-II algorithm was used to obtain the Pareto solution set. The technique for order preference by similarity to ideal solution (TOPSIS) was employed to select the appropriate optimal solution from the Pareto solution set. Chen et al. (2017) utilized the multi-index comprehensive balance analysis method to identify the parts with significant influence on crash outcomes. The body structures' thickness and material were optimized using a genetic algorithm, improving the vehicle body's energy absorption by 8.3% and reducing the weight by 33.32%. Jin et al. (2017) proposed a hybrid NSGA-II algorithm that obtains a more promising Pareto front than the original NSGA-II algorithm. The authors applied the hybrid algorithm to the process planning problem. Wang et al. (2016b) employed a multi-objective collaborative optimization method to minimize the vehicle body weight while maintaining crashworthiness.

Many studies combine several optimization algorithms to increase the optimization efficiency. For example, Afshinmanesh et al. (2005) proposed a new binary PSO method based on biological immune theory. Yildiz and Solanki (2012) combined the immune algorithm with PSO to filter and update PSO every 30 iterations, maintaining PSO's diversity. Comparison with existing algorithms proved the algorithm's suitability for complex engineering problems. In (Yildiz 2009), a hill-climbing local search was combined with the immune algorithm to improve the calculation efficiency

and avoid falling into a local optimum. Tan et al. (2014) integrated PSO and a new chaotic search method to solve the nonlinear integer and mixed-integer programming problems. Azzouz et al. (2017) tackled machine assignment and operation sequencing problems by proposing a hybrid algorithm that combines a genetic algorithm and an iterated local search.

Every optimization algorithm has not only its shortcomings (e.g., PSO's proneness to falling in a local optimum), but also unique advantages. Therefore, hybrid optimization algorithms emerged as a research trend in recent years. In a similar vein, this work develops a hybrid algorithm for SUV structure optimization. The main contributions of this paper are the following:

1. Building on the SUV rollover crashworthiness analysis, a multi-objective and multi-disciplinary SUV rollover crashworthiness and weight optimization is performed using the material structure integrated design method.
2. Radial basis function (RBF) neural network and a genetic algorithm are utilized to improve the overall accuracy of surrogate models describing the total weight, maximum contact force, and SUV structure's torsion frequency.
3. A hybrid optimization algorithm that combines particle swarm with artificial immune is proposed to enhance SUV rollover crashworthiness and minimize the weight. The algorithm mitigates PSO's limitations regarding the local optima susceptibility and reduces the artificial immune's computational cost.

The paper is organized as follows. In Section 2, the finite element (FE) SUV model is established and verified. The SUV's side and top body structures' contribution analysis highlights the parts critical for crashworthiness and weight. In Section 3, a multi-objective and multi-disciplinary SUV optimization problem is formulated. Section 4 establishes a surrogate model using the optimal Latin hypercube design (OLHD) method and RBF neural network. The surrogate model's accuracy is improved by utilizing a genetic algorithm to optimize the RBF neural network's hyperparameters. Section 5 introduces a hybrid particle swarm with the artificial immune optimization algorithm. The algorithm increases the solutions' distribution uniformity, diversity, and precision. Finally, Section 6 concludes the paper.

2 SUV rollover crashworthiness analysis and improvement

While SUV structure is complex, most components have little influence on rollover crashworthiness. This section analyzes the SUV components' contributions to rollover crashworthiness and weight and selects components essential for efficiency improvement and calculation cost reduction.

2.1 Finite element SUV model

In rollover accidents, the SUV's top structure plays a significant role in reducing passenger injury, especially to the head and neck of the human body. Therefore, NHTSA introduced FMVSS 216 to evaluate the vehicle roof structure's collapse resistance. The experimental method prescribed by FMVSS 216 is shown in Fig. 1.

Previous research utilized the FE method for roof crash simulation and determined the rigid plate speed could be set to 2235.2 mm/s. The maximum contact force between the rigid plate and vehicle roof could be as an important indicator of SUV rollover crashworthiness when the rigid plate moved forward within 127 mm (Walczak et al. 1999).

Figure 2a shows the NHTSA's FE SUV model. The US national collision analysis center carried out numerous crash simulations and proved the model's reliability in collision simulations (Jeong et al. 2008). The NHTSA's FE SUV model consists of 923 parts and includes 714,205 units and 724,628 nodes. However, many parts have little impact on SUV's rollover crashworthiness performance (e.g., chassis, wheels, engine, and SUV's interior). Therefore, the FE SUV model is simplified to reduce the calculation cost (Fig. 2b). The simplified model has 350,486 elements and 354,531 nodes, i.e., 50.93% and 51.07% reduction, respectively.

The SUV roof crash was simulated using the simplified model. The change in the contact force between the rigid plate and vehicle roof is shown in Fig. 3. Compared to the experiment results, the simulated contact force is only slightly reduced. The maximum simulated contact force is 46.7 kN, which is 1.68% less than NHTSA's results. Thus, the experiment verified the simplified model's validity in SUV rollover crashworthiness studies.

Fig. 1 FMVSS 216 experimental method

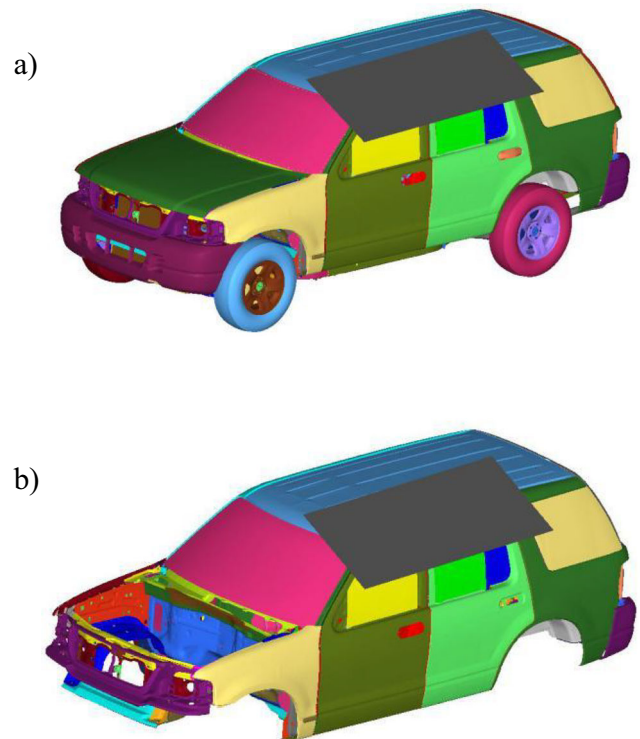
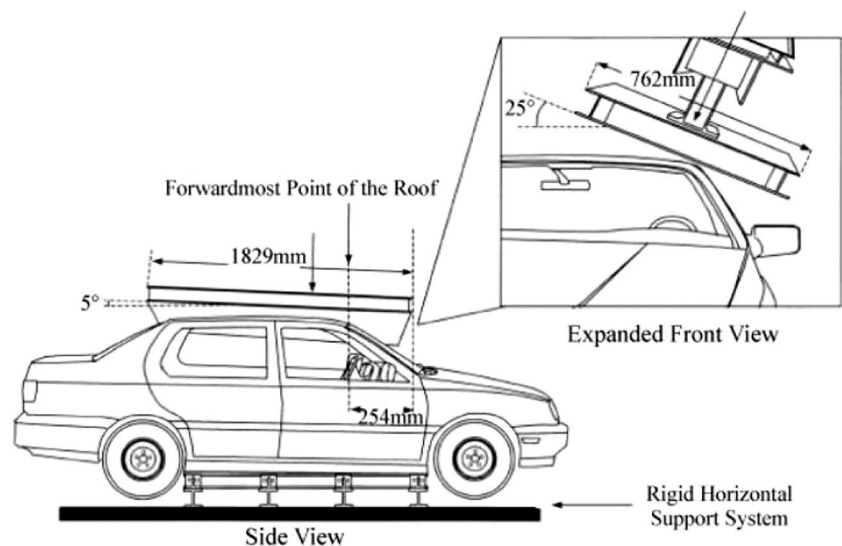


Fig. 2 FE SUV model. **a** NHTSA's SUV model. **b** Simplified SUV model

2.2 Contribution analysis of SUV structure components

Contribution analysis relies on statistics to determine the magnitude of each variable's influence on the performance, consequently enabling detection of components critical for the SUV rollover crashworthiness and weight.

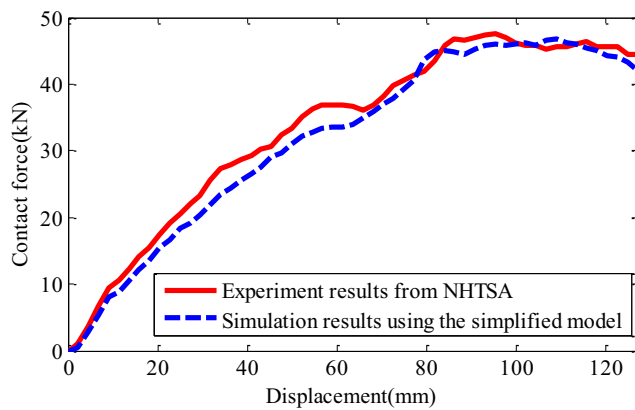


Fig. 3 Contact force between the rigid plate and vehicle roof

Linear contribution analysis determines correlations between component variables and rollover crashworthiness. The collected samples for each variable serve to establish a mathematical relation between input and output. Then, the approximate polynomial can be defined as:

$$f(x_1, x_2, \dots, x_N) = a + \sum_{i=1}^N \delta_i x_i + \sum_{i=2}^N \sum_{j=0}^{i-1} h_{ij}(x_i, x_j) + \varepsilon \quad (1)$$

where $f(x_1, x_2, \dots, x_N)$ is the objective function, N is the number of variables, a represents the total average value, h_{ij} is the interaction coefficient, and ε denotes the error. δ_i is the determined effect coefficient and represents the i^{th} variable's linear contribution. The variable's contribution to SUV performance (denoted CP_i) can be expressed as a percentage:

$$CP_i = \frac{\delta_i}{\sum_{i=1}^N |\delta_i|} \times 100\% \quad (2)$$

Due to the vehicle structure's symmetry (Fig. 4), thirteen components were selected for the contribution analysis. These components are significantly deformed during the rollover. Multivariate influence is analyzed using the orthogonal experiment method. The components' thickness is varied starting from the initial thicknesses given in Table 1. The variables range from 0.7 to 1.3 times the initial thickness. In this manner, three levels are obtained: the maximum, minimum, and initial thickness. Finally, an orthogonal table $L_{27} (3^{13})$ is generated.

Based on the $L_{27} (3^{13})$ table, 27 simulation experiment groups are conducted utilizing the simplified FE SUV model. The maximum contact force between the rigid plate and vehicle roof (F_{\max}) and the total SUV components' weight (W_s) are collected from each experiment. Furthermore, each component's contributions are obtained using (1) and (2) and shown in Fig. 5.

As seen in Fig. 5a, components C_1 and C_2 contribute over 20% to maximum contact force. Components C_3 , C_6 , C_7 , C_8 ,

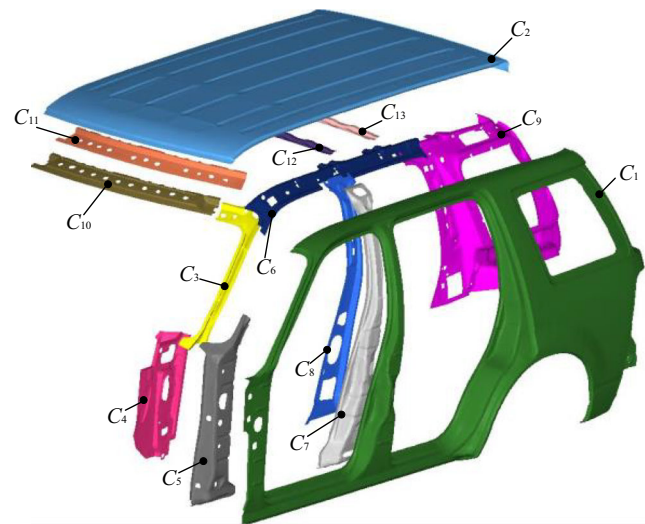


Fig. 4 SUV structure components considered in the rollover crashworthiness contribution analysis

and C_9 contribute over 4.5% each, whereas the remaining components' contributions are less than 3%. Thus, an increase in C_1 and C_2 thickness can greatly improve SUV rollover crashworthiness, but varying C_4 , C_5 , and C_{10} – C_{13} have a negligible impact.

Similarly, Fig. 5b shows that C_1 , C_2 , and C_9 each contribute over 7.8% to the total SUV components' weight.

2.3 SUV rollover crashworthiness improvement

The results in Section 2.2 show that modifying the A-pillar (i.e., component C_3) and B-pillar (composed of components C_7 and C_8) may improve SUV rollover crashworthiness. During SUV rollover, the severe bending deforms A- and B-pillars, but only a local yielding occurs. Therefore, reinforcing plates are added to the local yielding failure position to improve the component's bending resistance (Fig. 6). The reinforcing plates are made from high-strength steel with a yield limit of 480 MPa.

Next, SUV rollover simulations are repeated using the locally improved A- and B-pillars. The maximum contact force between the rigid plate and vehicle roof increased by 16.7% (i.e., to 54.5 kN), while the total SUV components' weight increased by 1.05 kg. These results show that the reinforcing plates improved SUV rollover crashworthiness to a limited extent but at the expense of an increase in the SUV's weight.

Since SUV components significantly influence the vehicle's dynamic performance, the excessive body mode change should be prevented. The body mode affects the ride comfort, especially the first-order torsion mode. Therefore, the vehicle body's torsion frequency (f_q) is selected to evaluate the SUV components' influence on ride comfort.

The original first torsion modal shape is shown in Fig. 7a. The torsion frequency is 33.45 Hz. The local A- and B-pillars' improvement has a small effect on the first torsion modal

Table 1 The components' initial thickness

Component	C ₁	C ₂	C ₃	C ₄	C ₅	C ₆	C ₇	C ₈	C ₉	C ₁₀	C ₁₁	C ₁₂	C ₁₃
Initial thickness (mm)	0.9	0.9	1.2	1.3	1.22	1	1.36	1.1	0.95	0.98	0.79	2.25	2.24

shape (Fig. 7b), where the obtained the first torsion frequency is 33.56 Hz. Thus, adding stiffeners to A- and B-pillars does not significantly hamper the ride comfort.

3 SUV rollover crashworthiness and weight optimization

The obtained improvements to SUV rollover crashworthiness are limited because C₃, C₇, and C₈ contribute to the maximum contact force far less than C₁, C₁₂, and C₉. The contribution analysis shows that, while increasing C₁–C₃ and C₆–C₉

thickness significantly improves crashworthiness, it also dramatically increases the total SUV weight. Thus, there is a trade-off between SUV rollover crashworthiness and weight. This section proposes a multi-objective optimization model that tackles this problem.

Following the conducted analysis, C₁–C₃ and C₆–C₉ components' thicknesses are selected as variables. In addition, since local improvements to A- and B-pillars increase the SUV rollover crashworthiness, the thickness of reinforcing plates added to A- and B-pillars may replace the C₃, C₇, and C₉ thickness. Thus, six design variables (denoted T₁–T₆) are selected for the parameters' optimization (Fig. 8).

Aluminum and magnesium alloys have been widely used in the automotive industry. Their use can greatly decrease SUV weight, improve static and dynamic performance, and promote crash safety. Table 2 shows the magnesium and aluminum alloys' mechanical properties. Following the conducted analysis (Fig. 5b), components' C₁, C₂, and C₉ yield strengths are selected as material variables (denoted M₁, M₂, and M₃, respectively), as shown in Fig. 8.

The objective function is defined with respect to W_s and 1/F_{max}. Several constraints are set to regulate the vehicle body's torsion mode and rollover crashworthiness. Formally, the multi-disciplinary and multi-objective optimization model for SUV rollover crashworthiness and weight is expressed as:

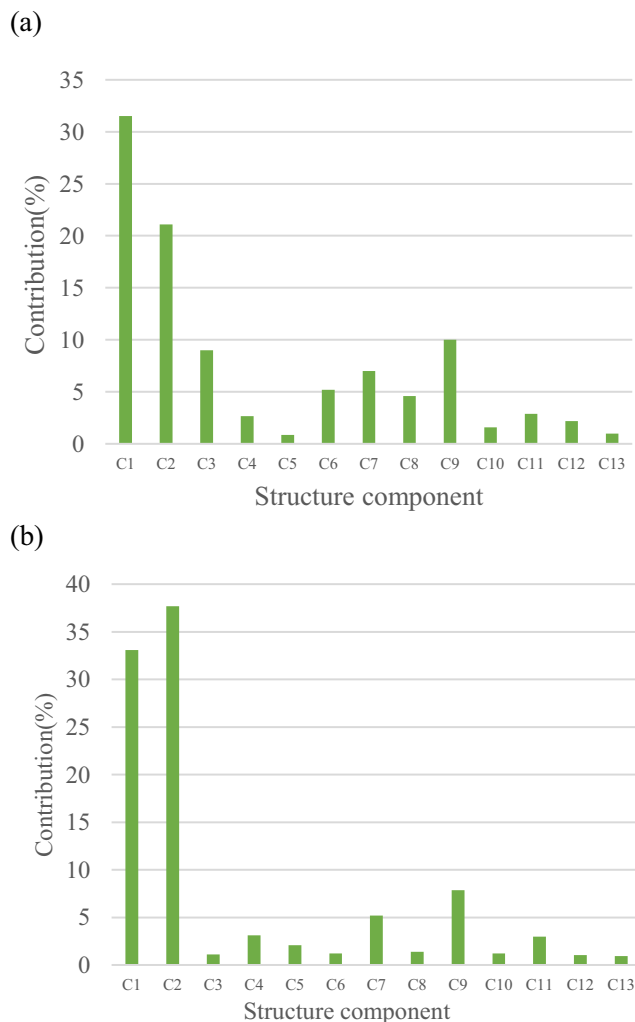


Fig. 5 SUV components' contribution to maximum contact force and total weight. **a** Maximum contact force. **b** Total weight

$$\left\{ \begin{array}{l} \text{find } (T_1, T_2, T_3, T_4, T_5, T_6, M_1, M_2, M_3) \\ \text{min } W_s, 1/F_{\text{max}} \\ \text{s.t. } 32.5\text{Hz} \leq f_q \leq 35.5\text{Hz} \\ F_{\text{max}} \geq 58.8\text{kN} \\ 1.4\text{mm} \leq T_1, T_2, T_3 \leq 2.2\text{mm} \\ 1.2\text{mm} \leq T_4 \leq 1.8\text{mm} \\ 1\text{mm} \leq T_5 \leq 1.6\text{mm} \\ 1.16\text{mm} \leq T_6 \leq 1.76\text{mm} \\ M_1, M_2, M_3 \in (\text{magnesium, aluminum}) \end{array} \right. \quad (3)$$

4 SUV rollover crashworthiness and weight surrogate model

Due to large deformations in SUV components, there is a strong nonlinear relationship between the components' parameters and crash performance, which cannot be easily expressed with formulae. By relying solely on the FE model to optimize the structural parameters, high calculation costs are obtained. RBF neural network has strong fault tolerance, robustness, adaptability, and ability to handle highly nonlinear

Fig. 6 Locally improved A-pillar and B-pillar. **a** Reinforcing plate added to A-pillar. **b** Reinforcing plate added to B-pillar

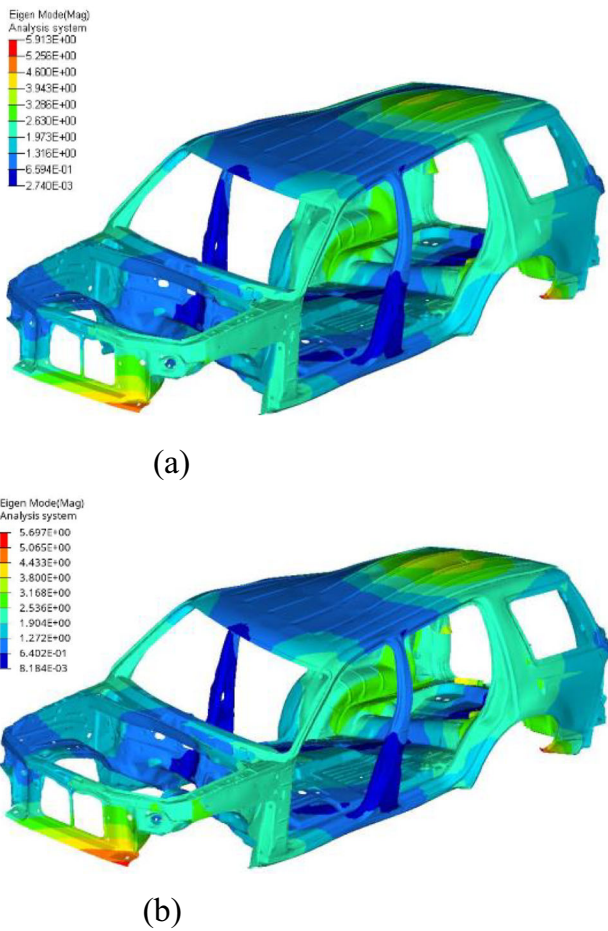
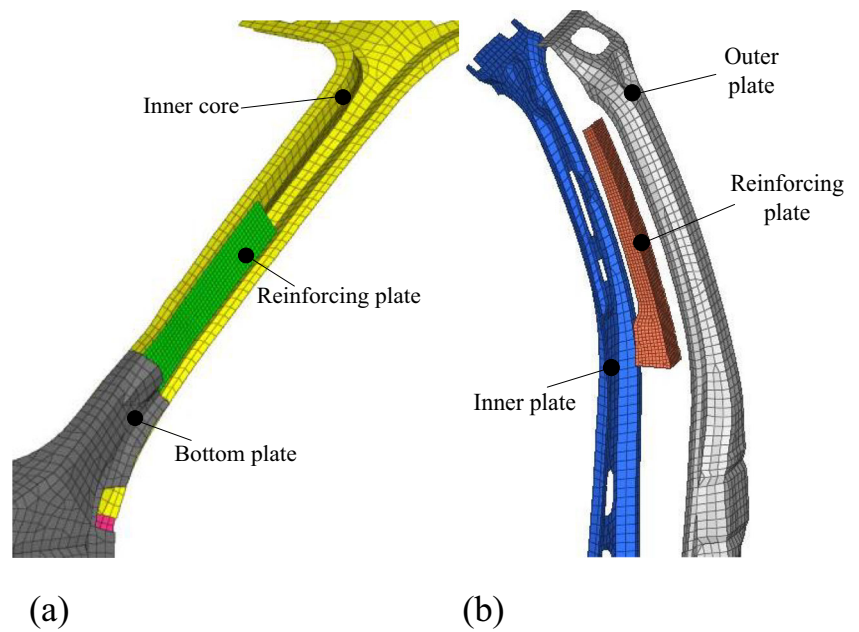


Fig. 7 The first torsion modal shape of SUV body. **a** Original SUV body. **b** Improved SUV body

problems. Thus, it is commonly employed to build surrogate models using mass, impact force, and mode (Wang et al. 2017). A similar approach is followed within this work. Since test data greatly affects the RBF neural network’s accuracy, the OLHD sampling method was used to generate 90 data groups, of which 75 were used to train the network’s weights and optimize the hyperparameters. The remaining data validated the surrogate model’s precision. To improve the forecast precision in the case of the limited samples, the RBF neural network’s hyperparameters are optimized using a genetic algorithm (Fig. 9).

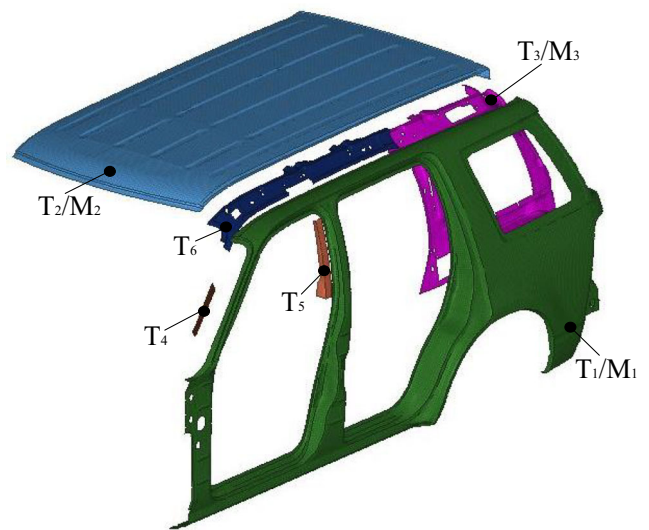


Fig. 8 Design variables for the multi-disciplinary and multi-objective optimization

Table 2 Magnesium and aluminum alloys' mechanical properties

Material	Density	Elastic modulus	Poisson ratio	Yield strength
Aluminum	2.7 g/cm ³	70GPa	0.3	189 MPa
Magnesium	1.82 g/cm ³	45GPa	0.3	160 MPa

4.1 A surrogate model based on RBF neural network

The RBF neural network's input layer takes a vector \mathbf{X} containing nine variables (T_1-T_6 and M_1-M_3). The output layer includes F_{max} , W_s , and f_q . The hidden layer has 75 nodes.

The input layer directly maps vector \mathbf{X} to the hidden layer. There is a nonlinear relationship between the input layer and the hidden layer and a linear mapping between the hidden and the output layers. Formally, the RBF neural network's output is obtained from the hidden layer as:

$$y_j = \sum_{i=1}^{n_m} w_{ij} \varphi_i(x) \tag{4}$$

where w_{ij} denotes the weight from the i^{th} neuron to the j^{th} output, and $\varphi_i(\mathbf{X})$ represents the radial basis function, i.e., the i^{th} neuron's activation. The radial basis function is defined using the Gaussian activation function:

$$\varphi_i = \exp\left(-\frac{1}{2\sigma^2} \|\mathbf{X}-S_i\|^2\right) \quad i = 1, 2, \dots, n_m \tag{5}$$

where σ is the Gaussian distribution's variance, S_i denotes the i^{th} neuron's Gaussian center, and n_m is the number of neurons in the hidden layer.

Throughout the training process, RBF neural network modifies the weights to improve the forecast precision. The error is calculated as:

$$E = \frac{1}{2t} \sum_{k=1}^t e_k^2 \tag{6}$$

$$e_k = \hat{y}_k - y_k \tag{7}$$

where E denotes the surrogate model's mean square error (MSE), y_k is the actual value, \hat{y}_k is the predicted value, and t denotes the number of samples.

The calculation steps are:

$$w_{(i+1)j} = w_{ij} - \eta \frac{\partial E}{\partial w_{ij}} \quad i = 1, 2, \dots, n_m \tag{8}$$

$$\frac{\partial E}{\partial w_{ij}} = \varphi_i(x) \sum_{k=1}^t e_k \tag{9}$$

where $\frac{\partial E}{\partial w_{ij}}$ is the error correction, and η is the learning rate.

Gaussian centers (S_i), variance (σ), and learning rate (η) greatly affect the RBF neural network's accuracy. S_i is obtained by collecting the evenly distributed samples from the sample space. Improper σ value increases the discrepancy between the predicted and the actual value. Learning rate η impacts the convergence speed and plays a key role when the sample is limited. Too large η prevents convergence, while a small η hampers learning. The surrogate model's errors are defined as (Yildiz and Solanki 2012):

$$R^2 = 1 - \frac{\sum_{k=1}^t (y_k - \hat{y}_k)^2}{\sum_{k=1}^t (y_k - \bar{y})^2} \tag{10}$$

$$e_{max} = \max\left(\frac{|y_k - \hat{y}_k|}{|y_k|}\right) \tag{11}$$

$$e_{RMS} = \sqrt{\frac{1}{t} \sum_{k=1}^t \frac{(y_k - \hat{y}_k)}{y_k}} \tag{12}$$

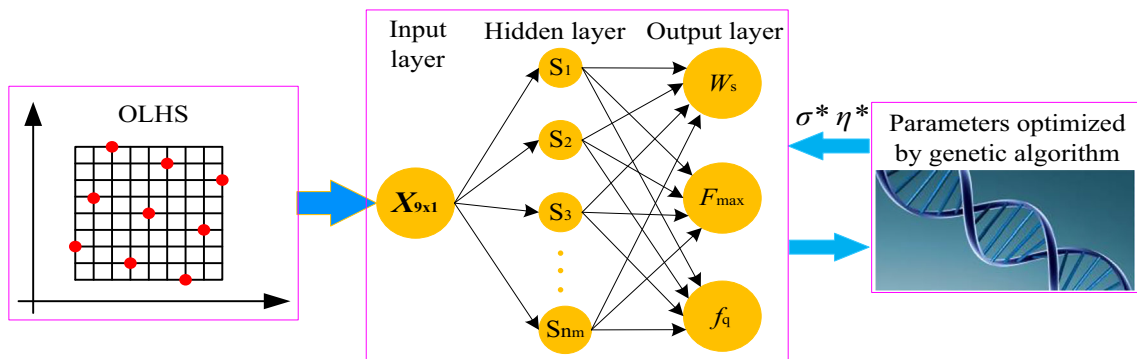


Fig. 9 The surrogate model's optimization flow chart

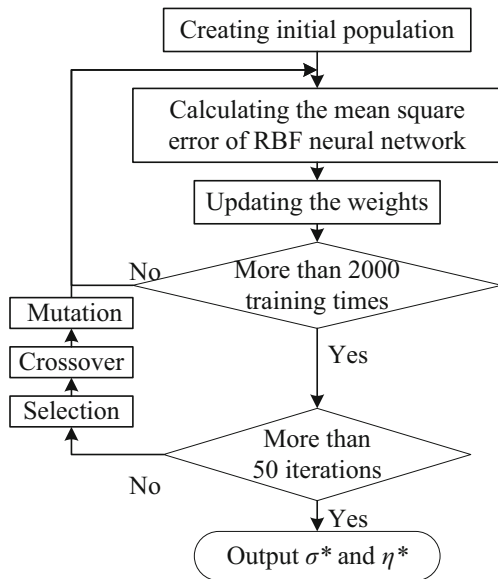
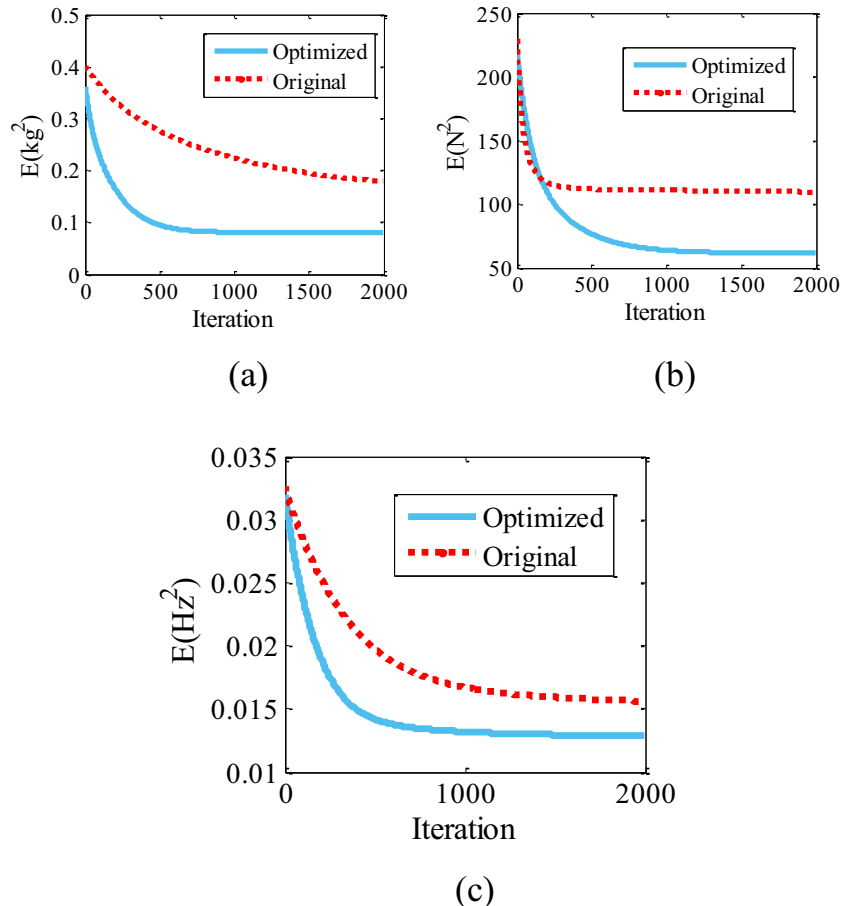


Fig. 10 Flowchart of the RBF neural network’s optimization using a genetic algorithm

where \bar{y} is the average value, R^2 denotes the surrogate model’s overall accuracy, and e_{\max} and e_{RMS} represent the surrogate model’s maximum error and root mean square (RMS) error.

Fig. 11 The surrogate model’s MSE. **a** Total weight. **b** Maximum contact force. **c** Torsion frequency



4.2 Parameter optimization using a genetic algorithm

As already noted, a genetic algorithm can optimize variance (σ) and learning rate (η) to improve the surrogate model’s accuracy. The optimization process is shown in Fig. 10. The RBF neural network’s loss function after training is used as the objective function. Next, 20 (σ, η) pairs are randomly generated within the variables’ range and taken as the initial population. The RBF neural network is established, and the weights are trained 2000 times to obtain a surrogate model. Ten (σ, η) pairs with the highest surrogate models’ accuracies are selected for crossover and mutation, generating 20 new (σ, η) pairs. After 50 iterations, the optimal pair (σ^*, η^*) is chosen.

4.3 Surrogate models’ accuracy analysis

Once established, the optimal parameters, σ^* and η^* , are used in the RBF neural network. Three optimal surrogate models can be considered: the maximum contact force surrogate model, the total weight surrogate model, and the torsion frequency surrogate model. Surrogate models’ MSEs are shown in Fig. 11, whereas their accuracy and maximum errors are given in Table 3.

Table 3 The surrogate models' accuracy comparison

Surrogate model		R^2	e_{\max}	e_{RMS}
W_s	Original	0.894	0.137	0.047
	Optimized	0.952	0.086	0.032
F_{\max}	Original	0.923	0.042	0.017
	Optimized	0.963	0.029	0.013
f_q	Original	0.873	0.114	0.031
	Optimized	0.931	0.066	0.019

Figure 11 shows that the RBF neural network (when optimized by the genetic algorithm) converges rapidly and significantly reduces the surrogate models' MSEs in the training process. In other words, the genetic algorithm improved the neural network's training efficiency.

The surrogate models' performance on the validation data was compared before and after optimization (Table 3). The overall accuracy increased by 6.5% for the total weight model, 4.3% for the contact force model, and 6.6% for the torsion frequency model. The maximum errors decreased by 37.2%, 31%, and 42.1%, and RMS errors decreased by 31.9%, 23.5%, and 38.7%, respectively. Thus, the optimization significantly improved the surrogate models' performance. The overall accuracy is over 0.9 for each model, while the maximum errors are less than 0.1.

5 Hybrid algorithm for SUV rollover crashworthiness and weight optimization

As previously emphasized, the considered objective function (defined in Section 3) has high dimensionality and strong nonlinearity. Furthermore, to minimize the objective function, the optimization method needs to solve three surrogate models iteratively and repeatedly screen, sort, clone, and mutate the intermediate results for nine variables. These characteristics pose significant requirements for the optimization method.

One candidate method is PSO. However, in addition to its previously noted limitations, once PSO converges, the particles may oscillate near the optimal solution, affecting the optimization accuracy. On the other hand, the artificial immune algorithm can enhance global convergence ability and restrain oscillations. However, when iteratively solving the three surrogate models, the artificial immune performs many complex calculations and reduces the optimization efficiency.

These two optimization algorithms can complement each other. Their combination may result in a more efficient optimization algorithm. Similar ideas were utilized in the existing research. For example, El-Sherbiny and Alhamalib (2013) used a mutation equation that considers antibody affinity to update the particle swarm flight speed. In Mahapatra et al. (2015), the gray image values are optimization targets. First,

PSO was utilized for optimization, and then affinity was used to screen the particle swarm for the optimal parameters. The selection strategy based on antibody density optimizes the speed update formula weights, consequently preventing the particle swarm's premature convergence (Du et al. 2016).

5.1 Particle swarm optimization

PSO is an intelligent optimization method that is based on the social behavior of particles' swarm. A suitable analogy is that of a bird flock. One particle can be regarded as a bird and the whole particle swarm as a group of birds looking for food. The optimal value is a spot with an abundance of food. In the initial state, the birds do not know where the food is, and they are randomly distributed. Each bird records the coordinates of the place where it found the food (individual optimal solution). In each iteration, the bird group records the optimum coordinates among the places visited by the birds (the global optimum). Each bird adjusts its flight path towards the global optimum (Hart and Vlahopoulos 2010; Cheng et al. 2012). In each iteration, particles' velocity and position are updated following the equations:

$$v^{i+1} = \omega^i v^i + \lambda_1 \text{rand}() \cdot [p_{\text{best}}^i - x^i] + \lambda_2 \text{rand}() \cdot [g_{\text{best}}^i - x^i] \quad (13)$$

$$x^{i+1} = x^i + v^{i+1} \quad (14)$$

where v^i and x^i are the i^{th} particle's current flight speed and position, p_{best}^i denotes the individual's optimal position, g_{best}^i represents the global optimal position, λ_1 and λ_2 are learning factors, and $\text{rand}()$ is a function that generates random numbers between 0 and 1. Thus, the particles' flight speed is affected by the global optimum, individual optimum, and current flight speed. If the current flight speed is too influential on the proceeding flight speeds, the particle vibrates around the optimal solution. In contrast, the lack of movement may affect the calculation efficiency. Therefore, the flight speed's weight should change over the iterations. Formally:

$$\omega^p = 0.9 - \frac{p}{p_{\max}} \times 0.5 \quad (15)$$

where p and p_{\max} denote current and the maximal number of iterations, respectively.

5.2 Artificial immune optimization algorithm

The immune algorithm is a new intelligent search algorithm inspired by a biological immune system. It is a heuristic random search algorithm, which combines certainty and randomness, enabling both exploration and exploitation (Carlos and Nareli 2005). The immune algorithm ensures population diversity by screening, cloning, and mutation. It has strong

global search ability and robustness (Alonso et al. 2014; Wakui et al. 2019).

The immune algorithm simulates the process of antibody recognition in an immune system to find the optimal solution. The optimization process includes affinity evaluation, antibody concentration evaluation, excitation degree evaluation, immune selection, cloning, mutation, clonal inhibition, and population renewal. Commonly, the objective function expresses affinity. Thus, the higher the function value, the higher the affinity. The antibody concentration represents the degree of antibody population aggregation and is formulated as:

$$\alpha_i = \frac{1}{n_c} \sum_{j=1}^{n_c} \mu(i, j) \tag{16}$$

$$\mu(i, j) = \begin{cases} 1, & d(i, j) < \gamma \\ 0, & d(i, j) \geq \gamma \end{cases} \tag{17}$$

where $\mu(i, j)$ denotes the similarity between the j^{th} and i^{th} antibodies. $d(i, j)$ represents the normalized distance between the j^{th} and i^{th} antibodies and is defined by (21). Finally, γ is the normalized distance threshold.

The antibody excitation degree can be obtained as:

$$\vartheta_i = \lambda_3 \zeta_i - \lambda_4 \alpha_i \tag{18}$$

where ϑ_i , ζ_i , and α_i denote the excitation degree, the affinity, and the i^{th} antibody's concentration, respectively. λ_3 and λ_4 are the weights.

Immune selection determines which antibodies should enter the cloning based on the antibodies' incentive degree. Highly motivated antibodies are more likely to be selected. Cloning copies the screened antibodies. The mutation adds a small disturbance to the clone, causing it to deviate from the original position and produce new antibodies. Clonal inhibition selects mutated clones, inhibits the low-affinity antibodies, and retains the high-affinity ones to enter the new antibody population. The low incentive antibodies in the population are deleted and replaced by new, randomly generated antibodies. New antibodies enter the next iteration. However, the immune algorithm's sorting and screening require multiple objective function evaluations, resulting in numerous calculations.

5.3 Hybrid algorithm combining PSO and artificial immune

A hybrid optimization algorithm that combines particle swarm with artificial immune is proposed to optimize the SUV components' parameters (Fig. 12). The hybrid optimization algorithm uses PSO to quickly search a group of non-dominated solutions on the Pareto front. Crossover operation is added to PSO. Each iteration randomly selects several particles for the variables' exchange. Such operation improves the population

diversity and prevents falling into a local optimum (Ardakan and Rezvan 2018). Then, artificial immune optimization restricts the uniform non-dominated solutions to a limited range to avoid oscillations.

The nine SUV components' variables, T_1-T_6 and M_1-M_3 , are selected as a group particle. The initial particle swarm is generated randomly. Each particle's objective function is calculated (i.e., W_s and F_{\max}) from three optimal surrogate models. New non-dominated solutions are obtained and punished by the penalty conditions, as follows:

$$W_s = 100, F_{\max} = 0 \\ \text{if } f_q > 35.5\text{Hz or } f_q < 33.5\text{Hz or } F_{\max} < 58.8\text{kN} \tag{19}$$

An external file is established to store the non-dominated solutions. The external file's capacity (n_c) is set to 60.

The density variance was introduced to evaluate the solutions' spatial distribution. Each particle's normalized total weight and maximum contact force are calculated as:

$$\begin{cases} \widehat{W}_s^i = \frac{W_s^i - \min(W_s^1, W_s^2, \dots, W_s^{n_c})}{\max(W_s^1, W_s^2, \dots, W_s^{n_c}) - \min(W_s^1, W_s^2, \dots, W_s^{n_c})} \\ \widehat{F}_{\max}^i = \frac{\widehat{F}_{\max}^i - \min(F_{\max}^1, F_{\max}^2, \dots, F_{\max}^{n_c})}{\max(F_{\max}^1, F_{\max}^2, \dots, F_{\max}^{n_c}) - \min(F_{\max}^1, F_{\max}^2, \dots, F_{\max}^{n_c})} \end{cases} \tag{20}$$

Then, the normalized distance and the density variance are defined:

$$d_i = \sqrt{\left(\widehat{W}_s^i - \widehat{W}_s^{i-1}\right)^2 + \left(\widehat{F}_{\max}^i - \widehat{F}_{\max}^{i-1}\right)^2} \quad i = 2 \dots n_c \tag{21}$$

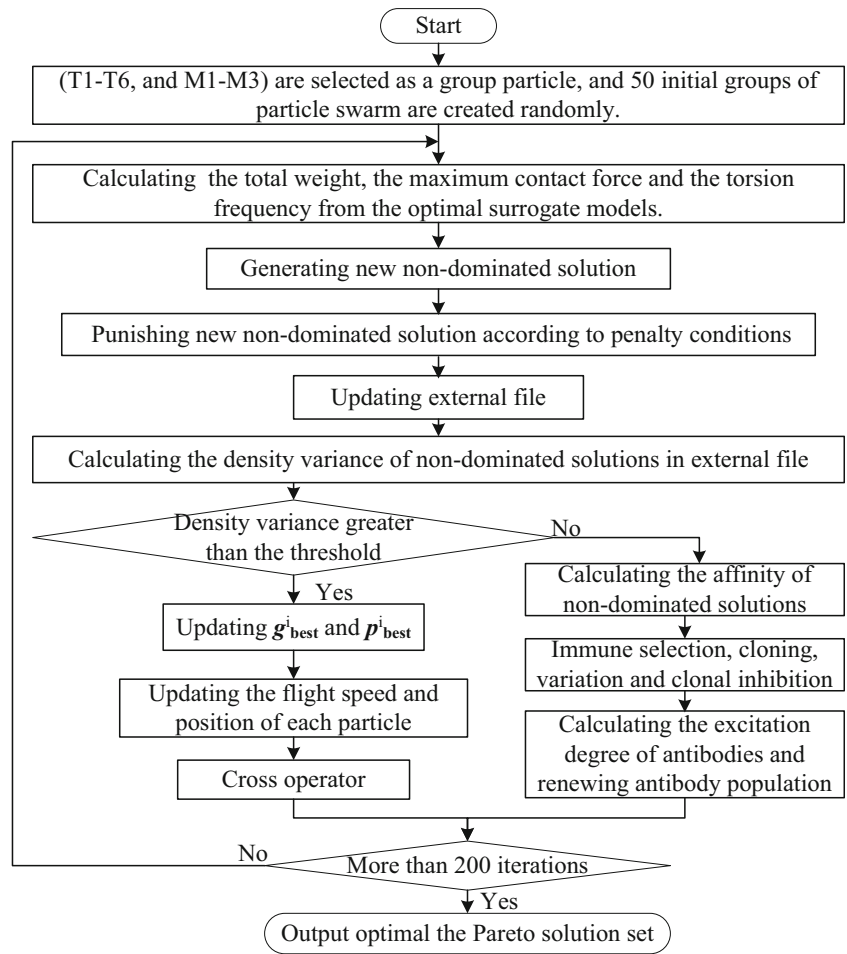
$$V_d = \frac{1}{n_c - 1} \sum_{i=2}^{n_c} [d_i - d_{\max} / (n_c - 1)]^2 \tag{22}$$

where V_d is the density variance, d_i denotes the normalized distance between the $(i-1)^{\text{th}}$ solution and the i^{th} solution, and d_{\max} is the maximum distance between non-dominated solutions.

When the number of non-dominated solutions exceeds the external file's capacity, the solution set is filtered. Small d_i means the short distance between the i^{th} solution and other surrounding solutions, i.e., a high solution density in the region. Thus, deleting the solution with small d reduces the calculation cost and ensures solutions' diversity.

Once the external file is updated, it contains 60 relatively scattered solutions. Then, the solutions' distribution is judged based on the density variance. If the distribution is not uniform (i.e., the density variance exceeds the threshold), the particle swarm performs a global search. In PSO, a global leader should be searched, but the external file solutions are not mutually dominated. Therefore, unlike single-objective optimization, multi-objective optimization cannot select a global optimum. To ensure solutions' diversity, the smallest density variance in

Fig. 12 Flowchart of hybrid optimization algorithm combined particle swarm with artificial immune



the external file is searched as the global leader solution. The fifth PSO optimization result is shown in Fig. 13.

Nine variables of one particle are exchanged with other particles to enhance PSO’s global search. The cross probability equals 0.8 and ensures population diversity.

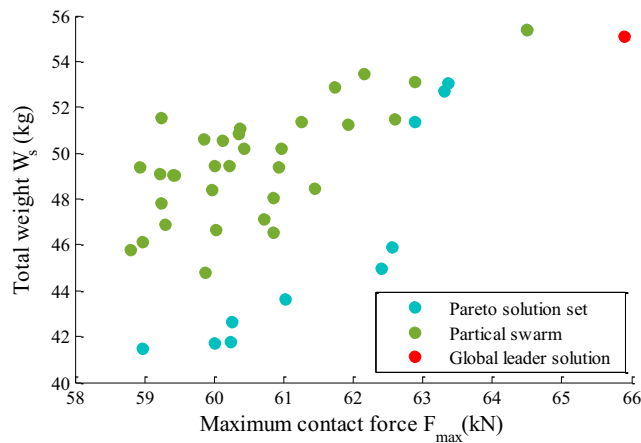


Fig. 13 The PSO’s results after five iterations

Suppose the solutions’ distribution in the external file is uniform (i.e., the density variance is smaller than the threshold). In that case, the artificial immune algorithm obtains an optimal solution by limiting the non-dominated solutions to vibrate in a small range. This mechanism prevents PSO oscillations around the optimal solution and reduces the computational cost.

The affinity function is constructed to generate initial antibodies and evaluate each antibody’s quality. Formally:

$$\zeta_i = -\widehat{W}_s^i + \widehat{F}_{\max}^i \tag{23}$$

The 25% of non-dominated solutions with the largest affinity in the external file are selected as initial antibodies (Fig. 14).

These new antibodies are immunized by sorting, screening, cloning, mutation, and inhibition cloning. To decrease the computational cost, the T_1-T_6 variables’ range is limited to 20% of the initial range. The antibody mutation rate is set to 0.7. Then, 60 antibodies are generated, and the antibodies with a large excitation degree (i.e., top 50%) are selected to renew

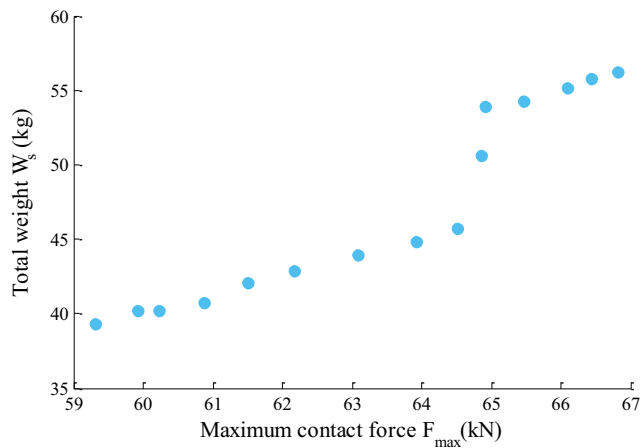


Fig. 14 Initial antibodies in artificial immune optimization

the external file. After 200 iterations, the optimal Pareto solution set is found.

5.4 Analysis of optimization results

Figure 15 shows the Pareto solution sets obtained using the hybrid optimization algorithm, immune algorithm, and PSO algorithm, respectively. The solutions obtained using the hybrid optimization algorithm are the closest to the Pareto front, indicating better SUV rollover crashworthiness and weight reduction. Furthermore, since the hybrid optimization algorithm utilizes density variance in solution selection, its Pareto solution set is more uniform than that of PSO or immune algorithm. The number of solutions obtained using PSO is 29, while the hybrid optimization and immune algorithms created 60. Due to its poor global search performance, PSO obtains fewer and less accurate Pareto solutions. The hybrid PSO algorithm uses a crossover operator to overcome this problem and shows strong global searchability. The immune algorithm has a high global searchability, but its convergence

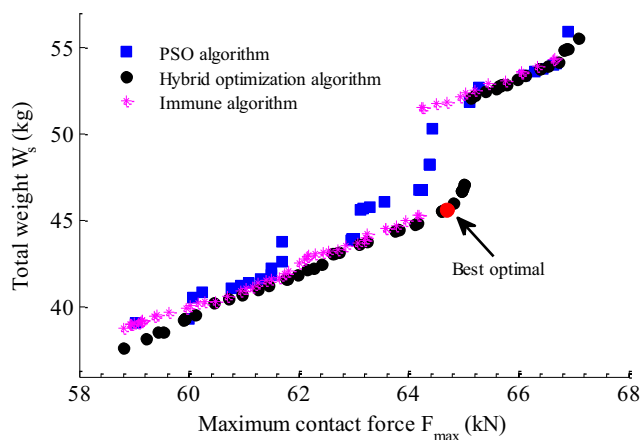


Fig. 15 The results for SUV rollover crashworthiness and weight optimization

is slow. The immune algorithm does not converge to a solution in the specified number of iterations. Consequently, its accuracy is suboptimal. Given the same number of iterations, the immune algorithm takes three times the proposed algorithm's computation time. The hybrid PSO algorithm employs PSO for the global search and then builds on the search results to reduce the subsequent antibody mutation range.

Therefore, the hybrid optimization algorithm effectively improves both PSO's and immune system's solutions' diversity, precision, and distribution uniformity.

None of the solutions in the Pareto solution set fully satisfies the requirements for SUV rollover crashworthiness, weight reduction, and ride comfort. Nevertheless, the Pareto solutions can be ranked using the TOPSIS method to determine the best compromise solution (Liang et al. 2018), as illustrated in Fig. 15. When the total weight reaches 47.07 kg, the Pareto solution set divides into two. Variable M_1 changes its value from Magnesium alloy in the first subset to Aluminum alloy in the second. M_1 is the material for the vehicle body's side and, since this area is large, a lot of material is required. Due to the difference in density between magnesium and aluminum alloy, the Pareto solution set shows a step phenomenon.

Table 4 shows the results for SUV rollover crashworthiness, weight reduction, and ride comfort. The hybrid optimization algorithm decreased the total SUV components' weight by 34.5%, while the maximum contact force between the rigid plate and vehicle roof increases by 18.7%. In other words, the hybrid optimization algorithm minimized the weight and improved the SUV rollover crashworthiness. In addition, the maximal first-order torsion frequency is 35.5 Hz, thus indicating no significant impact on the vehicle ride comfort.

6 Conclusions

This paper studied the SUV rollover crashworthiness and weight reduction through the lenses of structure components improvement and optimization.

The work analyzed the main structure components' contributions to SUV rollover crashworthiness and weight reduction. The influential factors' detection enabled the omission of less influential factors to increase optimization efficiency.

Table 4 The results for SUV rollover crashworthiness, weight reduction, and ride comfort

	W_s (kg)	F_{\max} (kN)	f_q (Hz)
Pre-optimized	69.6	54.5	33.6
Optimized	45.6	64.7	35.5

Based on the structure analysis, the influential parts are optimized, and crashworthiness is enhanced (the maximum contact force increased by 16.7%).

RBF neural network is optimized using a genetic algorithm and then applied to improve the accuracy of the surrogate models. The total weight surrogate model's accuracy improved by 6.5%, that of maximum contact force improved by 4.3%, and torsion frequency model's improved by 6.6%.

A multi-disciplinary and multi-objective model for SUV rollover crashworthiness and weight optimization is developed using the material structure integrated design method. A hybrid optimization algorithm that combines particle swarm with artificial immune is proposed. The algorithm takes full advantage of the PSO's fast convergence speed and uses PSO for global optimization. The crossover operator is added to PSO to enhance the PSO solutions' diversity and avoid falling into a local optimum. The non-dominated solution distribution is monitored and serves to adjust the next iteration's calculation method, consequently improving the optimization efficiency and reducing the calculation cost. Based on the selected non-dominated solutions, the variables' variation range is redefined, and immune operation is performed to generate the next-generation solutions. This algorithm effectively improves the local search ability, decreases the total SUV components' weight by 34.5%, and increases the maximum contact force between the SUV roof and rigid plate by 18.7%. That is, SUV rollover crashworthiness is enhanced significantly.

Acknowledgements The authors would like to thank anonymous reviewers for their valuable comments.

Funding This project is supported by the National Natural Science Foundation of China (Grant No. 51775269).

Declarations

Conflict of interest The authors declared that they have no conflict of interest.

Replication of results The results presented in this article can replicate by implementing the data structures and algorithms presented in the article. Because the codes of algorithms are not open source, the authors wish to withhold the code for commercialization purposes.

References

- Afshinmanesh F, Marandi A, Rahimi-Kian A (2005). A novel binary particle swarm optimization method using artificial immune system. In: IEEE international conference on computer as a tool, Eurocon, 217–220
- Alonso FR, Oliveira DQ, Zambroni AZ (2014) Artificial immune systems optimization approach for multiobjective distribution system reconfiguration. *IEEE Trans Power Syst* 30(2):1–8
- Arakan MA, Rezvan MT (2018) Multi-objective optimization of reliability–redundancy allocation problem with cold-standby strategy using NSGA-II. *Reliab Eng Syst Saf* 172:225–238
- Azzouz A, Ennigrou M, Said LB (2017) A self-adaptive hybrid algorithm for solving flexible job-shop problem with sequence dependent set-up time. *Procedia Comput Sci* 112:457–466
- Bai JT, Meng GW, Zuo WJ (2019) Rollover crashworthiness analysis and optimization of bus frame for conceptual design. *J Mech Sci Technol* 33(7):3363–3373
- Carlos AC, Nareli CC (2005) Solving multiobjective optimization problems using an artificial immune system. *Genet Program Evolvable Mach* 6:163–190
- Chen Y, Liu G, Zhang Z (2017) Integrated design technique for materials and structures of vehicle body under crash safety considerations. *Struct Multidiscip Optim* 56:455–472
- Cheng YM, Li L, Sun YJ et al (2012) A coupled particle swarm and harmony search optimization algorithm for difficult geotechnical problems. *Struct Multidiscip Optim* 45:489–501
- Choi W, Lee Y, Yoon J (2018) Structural optimization of roof crush test using an enforced displacement method. *Int J Automot Technol* 19(2):291–299
- Cui X, Zhang H, Wang S (2011) Design of weight reduction multi-material automotive bodies using new material performance indices of thin-walled beams for the material selection with crashworthiness consideration. *Mater Des* 32(2):815–821
- Deb K, Agrawal K, Pratap A, Meyarivan T (2000) A fast elitist non-dominated sorting genetic algorithm for multi-objective optimization: NSGA-II. *Lect Notes Comput Sci* 1917:849–858
- Du H, Liu DC, Zhang MH (2016) A hybrid algorithm based on particle swarm optimization and artificial immune for an assembly job shop scheduling problem. *Math Probl Eng* 2016:1–10
- El-Sherbiny MM, Alhamalib RM (2013) A hybrid particle swarm algorithm with artificial immune learning for solving the fixed charge transportation problem. *Comput Ind Eng* 64(2):610–620
- George R, John L, Gray S (1996) Rollover crash study-vehicle design and occupant injuries. 15th international technical conference on the enhanced safety of vehicles, Monash University Accident Research Centre, Report No. 65, Melbourne
- Gu X, Sun G, Li G (2013) A comparative study on multi-objective reliable and robust optimization for crash worthiness design of vehicle structure. *Struct Multidiscip Optim* 48:669–684
- Gundolf K, Elmar B, Roland S (2012) New weight reduction structures for advanced automotive vehicles safe and modular. *Procedia Soc Behav Sci* 48:350–362
- Hart CG, Vlahopoulos N (2010) An integrated multidisciplinary particle swarm optimization approach to conceptual ship design. *Struct Multidiscip Optim* 41:481–494
- Hou S, Liu T, Dong D (2014) Factor screening and multivariable crashworthiness optimization for vehicle side impact by factorial design. *Struct Multidiscip Optim* 49:147–167
- Jeong SB, Yi SI, Kan CD (2008) Structural optimization of an automobile roof structure using equivalent static loads. *Inst Mech Eng Part D: J Automob Eng* 222(11):1985–1995
- Jin H, Jin LL, Zhang CY (2017) Mathematical modeling and a hybrid NSGA-II algorithm for process planning problem considering machining cost and carbon emission. *Sustainability* 9(10):1769–1787
- Kennedy J, Eberhart R (1995) Particle swarm optimization. *IEEE* 1944:1942–1948
- Khalkhali A, Khakshourmia S, Nariman-Zadeh N (2014) A hybrid method of FEM, modified NSGAI and TOPSIS for structural optimization of sandwich panels with corrugated core. *J Sandw Struct Mater* 16(4):398–417
- Kiani M, Gandikota I, Rais-Rohani M (2014) Design of weight reduction magnesium car body structure under crash and vibration constraints. *J Magnes Alloys* 2(2):99–108

- Lee Y, Han Y, Park S (2018) Vehicle crash optimization considering a roof crush test and a side impact test. *Inst Mech Eng Part D: J Automob Eng* 233(10):2455–2466
- Liang D, Xu Z, Liu D et al (2018) Method for three-way decisions using ideal TOPSIS solutions at Pythagorean fuzzy information. *Inf Sci* 435:282–295
- Mahapatra PK, Ganguli S, Kumar A (2015) A hybrid particle swarm optimization and artificial immune system algorithm for image enhancement. *Soft Comput* 19:2101–2109
- Mohammad R, Sungmoon J, Jerzy W (2019) Rollover crashworthiness analyses an overview and state of the art. *Int J Crashworthiness* 24(2):1–23
- National Highway Traffic Safety Administration (NHTSA) (2018) Traffic safety facts 2016: a compilation of motor vehicle crash data from the fatality analysis reporting system and the general estimates system. US, Department of Transportation, Washington, DC, pp 70–77
- Perez RE, Behdinan K (2007) Particle swarm approach for structural design optimization. *Comput Struct* 85:1579–1588
- Tan Y, Tan G, Deng S (2014) Hybrid particle swarm optimization with chaotic search for solving. *J Cent South Univ* 21(7):2731–2742
- Trajkovski J, Ambroz M, Kunc (2018) The importance of friction coefficient between vehicle tyres and concrete safety barrier to vehicle rollover -FE analysis study. *J Mech Eng* 64(12):753–762
- Wakui T, Hashiguchi M, Sawada K et al (2019) Two-stage design optimization based on artificial immune system and mixed-integer linear programming for energy supply networks. *Energy* 170:1228–1248
- Walczak J, Guillermin O, Bathe KJ (1999) Advances in crush analysis. *Comput Struct* 72:31–47
- Wang D, Jiang R, Wu Y (2016a) A hybrid method of modified NSGA-II and TOPSIS for weight reduction design of parameterized passenger car sub-frame. *J Mech Sci Technol* 30(11):4909–4917
- Wang C, Wang D, Zhang S (2016b) Design and application of weight reduction multi-objective collaborative optimization for a parametric body-in-white structure. *Inst Mech Eng Part D: J Automob Eng* 230(2):273–288
- Wang J, Cai L, Zhao X (2017) Multiple-instance learning via an RBF kernel-based extreme learning machine. *J Intell Syst* 26(1):185–195
- Xiong F, Wang D, Ma Z (2018) Structure-material integrated multi-objective weight reduction design of the front end structure of automobile body. *Struct Multidiscip Optim* 57(2):829–847
- Yildiz AR (2009) A novel hybrid immune algorithm for global optimization in design and manufacturing. *Robot Comput Integr Manuf* 25:261–270
- Yildiz AR, Solanki KN (2012) Multi-objective optimization of vehicle crashworthiness using a new particle swarm based approach. *Int J Adv Manuf Technol* 59:367–376
- Zhu P, Zhang Y, Chen G (2009) Metamodel-based weight reduction design of an automotive front-body structure using robust optimization. *Proceed Inst Mech Eng Part D J Automob Eng* 223(9):1133–1147

Publisher's note Springer Nature remains neutral with regard to jurisdictional claims in published maps and institutional affiliations.